CONTINENTAL ICE BODY IN DOBŠINÁ ICE CAVE (SLOVAKIA) – PART II. – RESULTS OF CHEMICAL AND ISOTOPIC STUDY

Henrik Brink Clausen[1] – Kamil Vrana [2] – Steffen Bo Hansen[1] – Lars Berg Larsen[1] – – James Baker[3] – Marie-Louise Siggaard-Andersen[1] – Jesper Sjolte[1] – Sisse Camilla Lundholm[1]

[1] Ice and Climate Research Group, Niels Bohr Institute, University of Copenhagen, Juliane Mariesvej 30, DK-2100 Copenhagen

[2] Hydeko-KV, Planckova 4, 851 01, Bratislava, Slovakia

[3] Selor $_{EEIG}$, Saffierstraat 101c, 1074 GP, Amsterdam, The Netherlands

Abstract: This contribution continues information given in the workshop presentation K. Vrana et al. (2007) "Continental ice body in Dobšiná Ice Cave (Slovakia) – Part I. – project and sampling phase of isotopic and chemical study".

The main goal of this project is to investigate climatic and environmental changes by detailed study of continental cave ice using isotopic methods and methods of chemical analysis. According to existing knowledge we supposed that cores of cave ice from Dobšiná Ice Cave could add new information to the Holocene climate record of continental Europe. There are very only records of continental ice of similar type. Changes of climate are closely related to changes in the environment, so project results are supposed to be interesting from an ecological point of view, as well.

The Dobšiná ice body represents a dynamic system at a temperature close to the pressure melting point. The formation of the cave ice by various processes, like seeping and dripping groundwater, melting, refreezing, sublimation, condensation and evaporation, has formed the ice into a laminated block of frozen groundwater. Since the cave was discovered in 1870, comparison between old photos and drawings from the old times, and actual observations show that the distance from the ice surface at the Great Hall to the ceiling of the cave has been almost unchanged, meaning that the cave ice has been in a state of equilibrium for the last one and a half centuries.

The ice of the Dobšiná Ice Cave provides a unique opportunity to study a climatic record preserved in a continental European setting. The study encompasses continuous stable isotope (^{2}H and ^{18}O) and chemical analyses performed on samples from vertically drilled ice cores. The stable isotope (δD, $\delta^{18}O$) records are obtained by mass-spectrographic measurements. The chemical analyses include the water soluble ions: Na^+, K^+, NH_4^+, Mg^{2+}, Ca^{2+}, F^-, Cl^-, NO_3^- and SO_4^{2-}, and the concentration levels are determined by ion chromatographic measurements. For crystal size determination several thin sections have been taken along the ice cores and the crystal sizes recorded.

A prerequisite for using the stable isotope and the chemical records in palaeo-climatic studies is a time scale, a depth-age relationship for the ice core. A simple time scale for the cave ice has been established based on ^{14}C dating of a bat buried in the ice, and transported by the internal movement of the ice, from the surface at the Great Hall to the finding place in the ceiling of the Ruffiny's Corridor, 2.9 m above the bottom of the ice.

The interpretation of the stable isotope records in the sense of climatic information is not straight forward because the isotope ratios are affected by the high temperature and isotopic fractionation processes occur due to different processes like evaporation, melting and refreezing. Also the chemical components are affected by various processes like re-crystallization and removal of easy water soluble components from the ice.

The stable isotope ratios and the concentration levels of the chemical components in the laminated frozen ice body are compared with today's precipitation values from the region of the ice cave. The stable isotope ratios and the chemical data are compared to the crystal size and the visual stratigraphy determined by light transmission.

Key words: Dobšiná Ice Cave, drilling, ice core sampling, stable isotopes, chemical analyses

INTRODUCTION

From the Slovakian Dobšiná Ice Cave (DIC) a 14 m long ice core has been drilled from the icy floor in the "Great Hall". The ice core has been analysed for the stable water isotopes, $\delta^{18}O$ and δD, and soluble ions, Na^+, NH_4^+, K^+, Mg^{2+}, Ca^{2+}, F^-, Cl^-, NO_3^- and SO_4^{2-}. Also performed is analysis of crystal structures in thin sections. The ice contains air-bubbles in a large variety of sizes and structures. Some core sections show laminated structures,

while other sections appear very clear or very milky. The ion concentration levels vary along the core up to five orders of magnitude. Calcium is the lead component with concentrations exceeding 20 ppm or 1000 μequiv.·kg^{-1} (10^{-6} mole equivalent unit charge per kg of ice). Here we present the ice core record from the Dobšiná Ice Cave and discuss possible implications for the history of the cave in a palaeo-climatic perspective.

The first sampling expedition to the cave took place in June 2002, where the ice wall samples labelled Wall Site 1-3 have been collected (see Figs. 1 and 2 in Part I by Vrana et al., this volume). During the second sampling expedition in December 2002 three ice cores have been drilled, two of which, Core A and B, from the ice floor in the "Great Hall" close to the characteristic "Well", and one, Core C, vertically upwards from the bottom of the ice body. The samples represent ice from the uppermost part of the cave, close to the entrance (Wall Site 3), two parallel sections from the surface of the ice in the Great Hall (Core A and B) and three sections close to the base of the cave ice (Wall Site 1 and 2, and Ice Core C) (see Fig. 1, 3 and 5 in Part I by Vrana et al., this volume)

DATING OF THE ICE BODY

A time scale (age-depth relationship) is a prerequisite to interpret an ice core as regards to past climatic changes. Due to the high temperature of the ice (close to the pressure melting point) and the low accumulation rate, the traditional stable isotope methods can not be applied. We base our time scale on the observation that the surface of the ice body in the Great Hall to day shows an almost unchanged level compared to what is seen on old photography's and drawn pictures (Figs. 1 and 2) from the time when the cave has been found in the late nineteenth century. This indicates that the ice body has been in a state of equilibrium for the last 130 years.

A bat embedded in the ice of the ceiling in Ruffiny's Corridor has been transported by the internal movement of the ice from probably the surface of the Great Hall (949 m a.s.l.) to the finding place at 925 m a.s.l., 24 m below the floor of the Great Hall, and 2.9 m above the base level of the ice at 922 m a.s.l. (see Figs. 1, 2 and 6 in Part I. by Vrana et al., this volume). ^{14}C-dating has been performed on a piece of skin from the bat on the AMS-system at the Christian-Albrecht's University, Kiel, Germany (sample #KIA23374), and the Radio-Carbon age: 1168 ± 28 BP corresponds to a calibrated age: AD 888 ± 73/109 (Fig. 3). Holmlund et al. (2005) report similar ^{14}C-ages for wooden material found in a Romanian cave ice. Assuming equilibrium for the ice body during the last millennium (as observed for the last century) we find a mean vertical velocity and an average yearly rate of accumulation: 2410/1114 = 2.16 cm per year. An estimate of the horizontal velocity depends upon the site at the surface where the bat has been frozen in. The horizontal distance from a position in the central part of the Great Hall to the finding place of the bat in Ruffiny's Corridor is approximately 30 m, corresponding to a horizontal velocity of 3000/1114 = 2.7 cm per year. These values are within the ranges

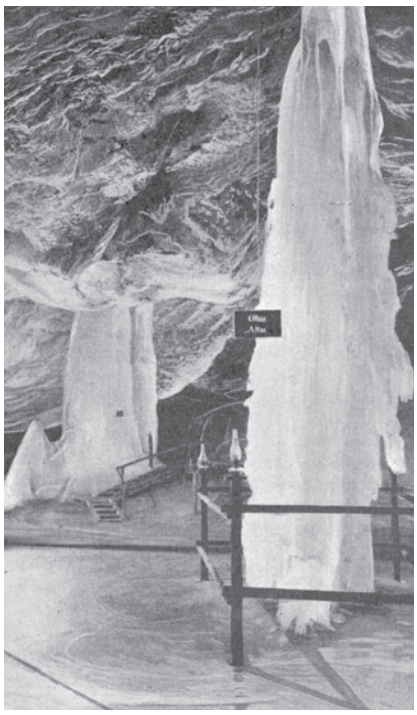

Fig. 1. The picture shows the two characteristic ice features of the Great Hall, the Well and the Alter. The image is from Ede (1908), fig. 1 on page 9. Ice Core A has been drilled in front of the Well approximately where the descending wooden staircase ends. The drilling ended when the drill hits wood at a depth of 1.6 m.

Fig. 2. The picture shows the Well and the Alter in 2002 seen from the opposite side of Fig. 1.

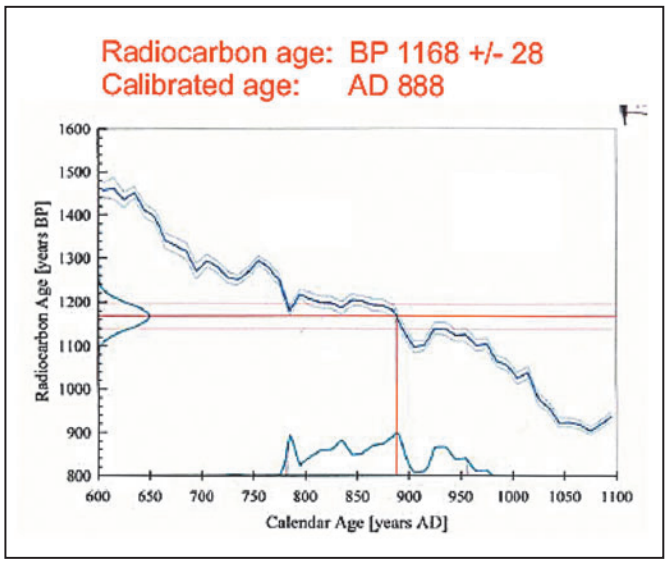

Fig. 3. The actual measured radiocarbon age with ± 1σ uncertainty is plotted on the ^{14}C-calibration curve (InterCal98). The lower curve exhibits the probability within the ±1σ range.

of velocities reported by Lalkovič (1995): vertical movements 0.15 – 7.85 cm per year and horizontal movements 0.54 – 1.81 cm per year. Using a simple time scale, assuming a constant annual rate of accumulation 2.16 cm per year, we obtain for the three ice cores:

Core	Length, m	Δ years	Time span, AD
A	1.61	75	1927 – 2002
B	13.93	645	1357 – 2002
C*	0.93	43	845 – 888
Ice body	27.0	1250	745 – 2002

C* The bottom of this core is approximately 2 m above the bottom level 922 m a.s.l. (see Fig. 1 in Part I by Vrana et al., this volume).

SAMPLING

Immediately after recovery, the ice cores and wall samples are documented and packed in insulated foam boxes for transportation in the frozen state to the ice core laboratory at the Niels Bohr Institute in Copenhagen, where further sampling and analyses take place. The sample resolution for isotope and chemistry measurement is 5 cm for the ice wall samples, labelled Wall Site 1, 2 and 3 (see Part I by Vrana et al., this volume), and 2.5 cm in the case of the ice cores labelled Core A, B and C. All three ice cores have been thoroughly photographed with a digital camera for visual investigations.

Sampling for isotopes is performed with a band saw while decontamination and sampling for chemical analyses are performed manually with a microtome knife in a laminar flow bench placed in the cold laboratory at –14 °C. The samples for chemistry analyses are stored frozen in Coulter accuvettes until immediately before measurements.

ANALYSES

ISOTOPE MEASUREMENTS

The ice samples for the stable isotope analyses are melted and the $\delta^{18}O$ are measured on a semi-automatic mass spectrometer at the Niels Bohr Institute. Residual sample volumes are sent to the AMS ^{14}C Dating Centre at the University of Aarhus and measured for δD using a Continuous-Flow Isotope Ratio Mass Spectrometer (Morrison et al., 2001). The measuring accuracy of the individual samples is 0.07 and 0.5 per mil for $\delta^{18}O$ and δD, respectively.

CHEMISTRY MEASUREMENTS

The frozen pre-cleaned ice samples are taken to a clean room at the Niels Bohr Institute, where they are melted and decanted into pre-cleaned 5 ml vials for ion chromatographic (IC) analyses of water soluble ions. The samples are analysed simultaneous for anions (F^-, Cl^-, NO_3^-, and SO_4^{2-}) and cations (Na^+, K^+, NH_4^+, Mg^{2+}, and Ca^{2+}) in a two channel IC set-up, consisting of two Dionex 500 microbore systems. The wall site samples 1, 2 and 3 from the pilot study are analysed using 10 µl and 25 µl sample loops, respectively in the anion and the cation system. For the analysis of the ice cores A, B and C the sample loops are changed to 100 µl for both systems in order to optimise the measurement of samples with differences in concentration levels of up to five to six orders of magnitude. The effect of this change is clearly seen in Table 2 (see later in text). Uncertainties, estimated from repeated measurements of a standard solution, vary for the different elements (see Table 1).

*Table 1. Typical analytical uncertainties in per cent of measured value determined by repeated measurements of standard solutions. *The high uncertainty in the case of Mg^{2+} is mainly due to the difficulty in separating the Mg^{2+} peaks from the Ca^{2+} peaks with high concentration levels.*

Element	per cent
Na^+	1.5 – 8
NH_4^+	1.5 – 4
K^+	1.5 – 8
Mg^{2+}	11 – 17*
Ca^{2+}	2 – 3
F^-	1 – 1.5
Cl^-	1 – 2
NO_3^-	2.5 – 4
SO_4^{2-}	1 – 2.5

CRYSTAL ANALYSES

A total of 27 vertical slices of ice from the ice wall 1, 2 and 3 (3 pcs.), and from the ice cores A (2 pcs.), B (21 pcs.) and C (1 pc.) are prepared for visual crystal size analyses. The ice slices (7 – 10 cm long and 0.5 cm thick) are planed smooth to a thickness of 0.5 mm using a Leica thin cutter with a microtome knife. These thin sections are placed in a Rigsby stage between two crossed polarizing filters, which make the crystals appear in different colours dependent upon their crystal orientation.

Table 2. The table exhibits mean values and minimum to maximum ranges of $\delta^{18}O$, δD and d (top 3 double rows) and similar values of the concentration levels of Na^+, NH_4^+, K^+, Mg^{2+}, Ca^{2+}, F^-, Cl^-, NO_3^- and SO_4^{2-} (bottom 9 double rows) from Ice Wall Site 1, 2 and 3, and Ice Core A, B and C, and 1.6 m top part of Core B, and 2 m bottom part of Core B. The lowest 13 m of the ice body is represented by Wall Site 2, Core C and Wall Site 1 comprising a total of 3.2 m of the 4.7 m bottom part, meaning that a depth interval of some 8.3 m is not represented by any ice samples. The parentheses around the Ice Wall Site samples mean that samples with low concentration levels can not be detected due to the applied measuring method (see text). This is clearly seen in the ranges where only the upper limits fit those from the ice cores. The only exception from this is seen in the Ca^{2+} values of Ice Wall Site 2, here all values are above the limit of detection. In the case of Ice Wall Site 1 all NO_3^- values are below the line of detection (see text).

	Ice Wall 3 DIC023 1.31 m	Core B DIC02B 13.92 m	Core B DIC02B Top 1.6 m	Core A DIC02A 1.61 m	CoreB DIC02B Bottom 2 m 11.0 – 13.9 m	Ice Wall 2 DIC022 1.21 m	CoreC DIC02C 0.93 m	Ice Wall 1 DIC021 1.07 m
δ^{18} O per mil								
Mean	-10.32	-8.39	-8.24	-8.30	-9.33	-9.24	-8.51	-7.68
Range	-14 to -9	-12 to -6	-12 to -6	-11 to -7	-11 to -8	-10 to -8	-9 to -8	-8 to -7
δD per mil								
Mean	-70.37	-58.91	-55.36	-56.53	-63.10	-62.26	-57.48	-50.42
Range	-97 to -58	-79 to -39	-78 to -41	-78 to -44	-73 to -50	-67 to -57	-64 to -53	-55 to -48
d per mil								
Mean	12.22	11.34	10.57	9.91	11.54	11.64	10.57	11.01
Range	10 to 15	9 to 15	9 to 15	8 to 12	10 to 13	10 to 13	9 to 12	10 to 13
Na^+ µeq/kg								
Mean	(43.9)	5.84	2.39	2.63	2.48	(33.4)	2.51	(25.0)
Range	(13.4 – 69)	0.03 – 446	0.28 – 16	0.09 – 47	0.003 –16	(1.47 – 167)	0.38 – 16	(0.62 – 47)
NH_4^+ µeq/kg								
Mean	(27.8)	2.58	1.67	2.15	2.58	(2.07)	0.74	(1.52)
Range	(8.0 – 59)	0.003 – 58	0.26 – 11	0.016 – 29	0.007 – 12	(0.37 – 8.3)	0.01 – 8.2	(0.27 – 3.4)
K^+ µeq/kg								
Mean	(18.6)	0.99	0.64	0.44	1.71	(3.75)	0.80	(2.00)
Range	(7.8 – 35)	0.001 – 82	0.09 – 2.9	0.012 – 2.5	0.001 - 25	(0.29 – 21)	0.006 – 6.0	(0.08 – 9.0)
Mg^{2+} µeq/kg								
Mean	(64.2)	2.96	2.37	0.86	5.24	(4.86)	2.17	(2.56)
Range	(27 – 125)	0.001 – 109	0.04 – 31	0.012 –4.0	0.001 – 80	(1.34 – 14)	0.005 – 6.8	(0.71 – 6.5)
Ca^{2+} µeq/kg								
Mean	(724)	235	205	213	360	275	692	(240)
Range	(457 – 1240)	0.006 – 1314	27 – 693	29 – 765	0.006 – 1314	159 – 376	443 – 916	(104 - 347)
F^- µeq/kg								
Mean	(2.03)	0.18	0.18	0.27	0.12	(8.37)	0.18	(5.03)
Range	(1.4 – 7.3)	0.017 – 0.69	0.05 – 0.43	0.13 – 0.76	0.05 – 0.36	(3.3 – 21)	0.12 – 0.24	(1.8 – 9.1)
Cl^- µeq/kg								
Mean	(68.3)	7.67	3.60	4,15	7.49	(35.0)	3.89	(22.4)
Range	(16 – 127)	0.006 – 536	0.38 – 18	0.32 – 24	0.16 – 60	(1.3 – 187)	0.09 – 74	(1.1 – 42)
NO_3^- µeq/kg								
Mean	(3.18)	2.57	3.15	1.57	3.97	(6.29)	0.55	(no values)
Range	(1.8 – 6.4)	0.001 – 52	0.04 – 32	0.19 – 8.1	0.001 – 52	(2.0 – 16)	0.001 – 5.0	
SO_4^{2-} µeq/kg								
Mean	(38.0)	43.8	50.5	19.8	10.5	(6.87)	7.35	(2.76)
Range	(5.1 – 87)	0.006 – 445	2.2 – 362	0.04 – 159	0.14 – 187	(1.2 – 22)	3.4 – 19	(1.2 – 8.1)

RESULTS

ISOTOPES

The composition of stable water isotopes in the ice is reported using the δ-function as the relative sample deviation from the Vienna Standard Mean Ocean Water (SMOW) in the unit per mil. In addition to the $\delta^{18}O$ and δD isotope values we obtain a second order parameter, the deuterium excess, **d** = δD - 8 · $\delta^{18}O$ (Dansgaard 1964).

The upper three rows of Table 2 summarize the mean δ-values and the ranges for the various sample collections in the unit per mil. The samples show large variability of both the δ- and the **d**-values. Fig. 4 shows δD plotted against $\delta^{18}O$ for the cores A and C, and the Wall Sites 1 and 3 together with winter values from various locations in the mountain areas in the vicinity of the Dobšiná Ice Cave (Fig. 5), (Michalko, 1999). The data shows a linear relationship between the two parameters (δD = 7.66 · $\delta^{18}O$ + 7.67) very close to the Global Meteoric Water Line (GMWL) δD = 8 · $\delta^{18}O$ + 10 (Craig, 1961), which means that the accumulated cave ice originates from precipitation, and this indicates that there may be a climate signal in the isotopes.

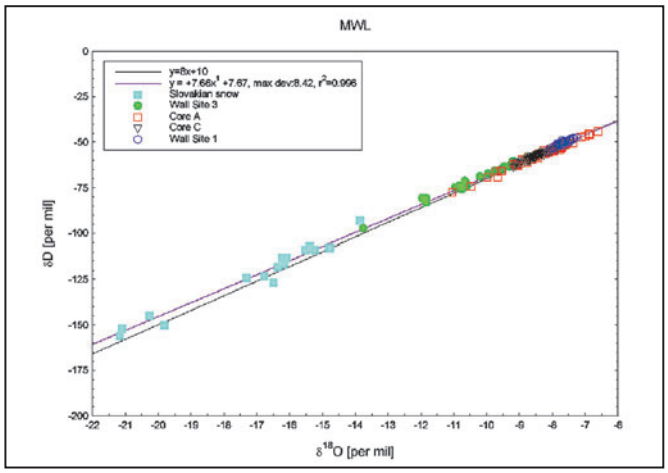

Fig. 4. The figure presents a meteoric water line (MWL) for the region around the Dobšiná Cave. The MWL is based on δ-values from cave ice and Slovakian snow samples.

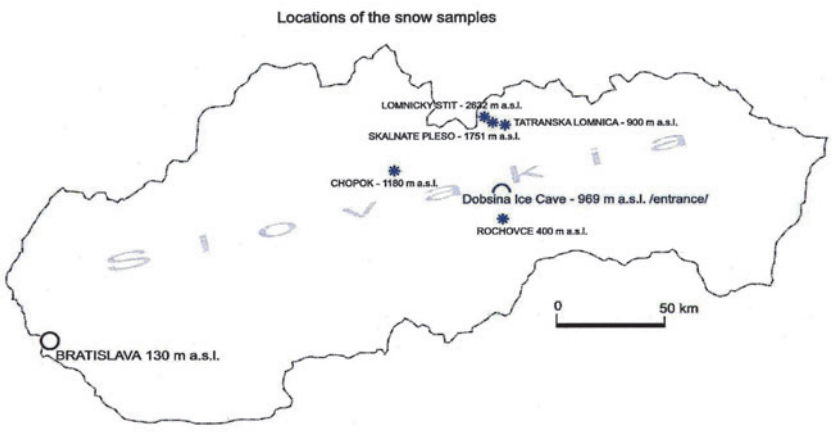

Fig. 5. Slovakian snow sampling sites for $\delta^{18}O$ measurements (according to Bodiš et al. 2000)

Compared to the δ values of precipitation collected in mountain areas in the vicinity of the Dobšiná Ice Cave, the δ values for the cave ice are much less depleted. The average $\delta^{18}O$ value of the 64 samples that comprises Core A is -8.30 per mil. These samples represent the last approximately 75 years of accumulation in the cave according to the preliminary simple age model. For the surrounding area within a radius of about 150 km (Fig.5), the annual mean $\delta^{18}O$ values are between -10.44 and -9.09 per mil (Michalko, 1999). The altitude effect, estimated to be 0.1 per mil per 100 m, is small, so a comparison is feasible. The less depleted δ values of core A indicate that a substantial part of the net accumulation of ice in the cave happens during the rainy seasons in spring and autumn when the temperatures are higher than during the winter season where the precipitation samples has been taken.

In the cave ice the deuterium excess, **d**, is generally negatively correlated to $\delta^{18}O$, although the phase at some depths is slightly positively or negatively offset. The reason for the negative correlation between **d** and $\delta^{18}O$ lies in the fact that the δD versus $\delta^{18}O$ relation has a slightly lower slope than the GMWL which is the basis for the **d**-definition. The δD versus $\delta^{18}O$ slope in Core B changes from about 7.37 ± 0.07, in the top 3.125 m, to about 7.64 ± 0.04 deeper in the core (see Table 3). The different δD versus $\delta^{18}O$ slopes are reflected in the amplitude of the **d**-variations, where periods of smaller slope are associated with a more pronounced negative correlation between $\delta^{18}O$ and **d** with larger amplitudes.

Table 3. The table shows the linear fit of δD versus $\delta^{18}O$ for two depth intervals 0 – 3.215 m and 3.125 – 13.93 m. The depth level 3.125 m corresponds to approx. AD 1860 (see text) and at this depth is observed a clear change in the $\delta^{18}O$ pattern from a high frequency type of oscillation to a low smooth type (see Fig. 11).

Depth interval	Linear fit of δD versus $\delta^{18}O$
0 – 3.125 m	δD = 7.37 (± 0.07) · $\delta^{18}O$ + 5.25 (± 0.62)
3.125 – 13.93 m	δD = 7.64 (± 0.04) · $\delta^{18}O$ + 8.36 (± 0.34)

The different slopes can be caused by changes in evaporative conditions outside as well as inside the cave. Outside the cave a general change of the precipitation conditions during precipitation in the area affects the δD versus $\delta^{18}O$ slope (Liebminger, 2006). The sub cloud evaporation is dependant on the relative humidity, as less relative humidity enhances the evaporation and results in a lower slope of the local MWL. Changing evaporative conditions for collected water inside the cave can also affect the δD versus $\delta^{18}O$ slope, as observed in the case of lake water (Gibson, 2002). The governing accumulation process in the DIC is freezing of liquid water onto the existing ice. A change in the isotopic composition

of the water occurs during evaporation before the water freezes and increased evaporation in the cave will result in a decreased δD versus $\delta^{18}O$ slope.

The top 3 m of Core B spans the past approximately 140 years according to the simple age model. This time span coincides with the period when a part of the cave wall, near the present cave entrance was modified to provide access to the cave. The enlargement and modification of the ceiling and related cave walls affected the air flow in the cave. This may be the reason for the change in slope, as increased evaporation in the cave after the cave entrance modifications can have resulted in the observed lower δD versus $\delta^{18}O$ slope.

Table 4 presents the $\delta^{18}O$ mean values of 7 sections (a-g) from Core B and mean values for Wall Site 1, 2 and 3, and Core A and C, and top and bottom parts of Core B. The data are presented in Fig. 6 on a depth scale with zero depth level at Wall Site 1 to show a possible effect of the Arnason fractionation process (Arnason 1969). Because the temperature of the ice mass is close to the melting point, there is an interaction between frozen ice and melt water and we can expect changes in the stable isotope composition of the ice due to fractional processes e.g. the so called Arnason effect, which results in depletion of heavy isotopes in the melt water and an enrichment of heavy isotopes in the ice. Fig. 6 shows that the $\delta^{18}O$ values of Core B (blue circles) has not suffered from this process (negative trend) whereas the Wall Site samples show the opposite trend, especially Wall Site 3 with a one per mill higher value than Core C from almost the same depth at the bottom of the ice.

Table 4. Mean $\delta^{18}O$ and standard deviation values of 7 sections (a – g) from Core B and of 7 sampling sites (Wall site 1, 2 and 3, Core A, Top of Core B, Bottom of Core B and Core C) are presented on various depth scales for use in Figs. 6, 8 and 9 (se text).
** Level at surface for Core B and A 949.78 and 949.00 m a.s.l., respectively.*
*** Zero depth level at Wall Site 3, 958 m a.s.l. (see Fig. 1 in part I by Vrana et al., this volume).*

Site and section	Depth at bottom of sample, m	Sample level* m.a.s.l	Depth below Site Wall 3** m	Mean $\delta^{18}O$ per mil	Std $\delta^{18}O$ per mil
Core B, a	2	947.78	10.22	-8.40	1.28
Core B, b	3.025	946.76	11.25	-9.21	0.71
Core B, c	5.7	944.08	13.92	-8.17	0.91
Core B, d	8.187	941.59	16.41	-8.58	0.81
Core B, e	10.9	938.88	19.12	-9.11	0.53
Core B, f	12.7	937.08	20.92	-9.06	0.57
Core B, g	13.92	935.86	22.14	-9.68	0.31
Wall Site 3	(1.31)	958.00	0.00	-10.32	1.13
Core B, (top)	1.6	948.18	9.82	-8.05	1.05
Core A	1.61	947.39	10.61	-8.30	0.85
Core B, (bot)	11.9 – 13.9	935.86	22.14	-9.33	0.62
Wall Site 2	(1.21)	925.50	32.50	-9.24	0.35
Core C	(0.93)	924.00	34.00	-8.51	0.33
Wall Site 1	(1.07)	922.00	36.00	-7.68	0.21

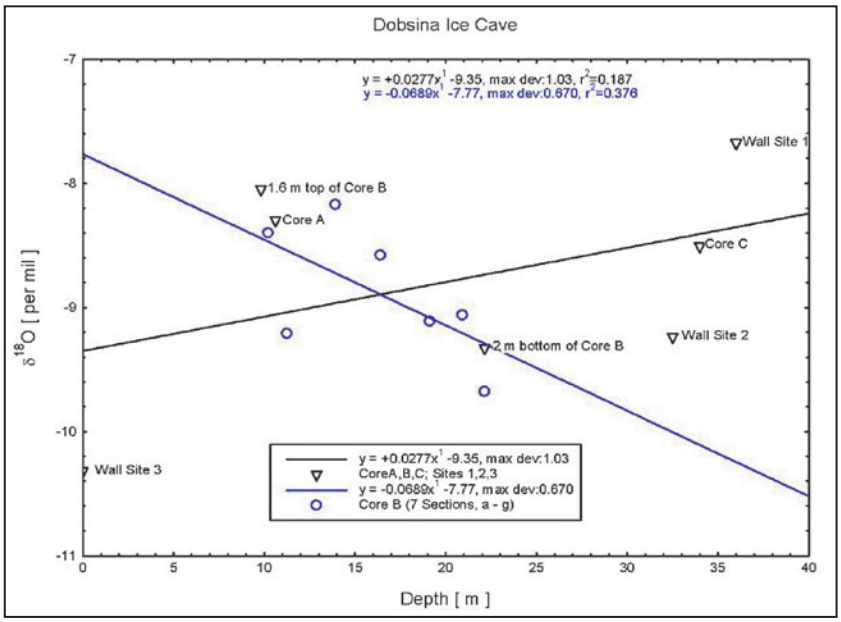

Fig. 6. The $\delta^{18}O$ values of the 7 sections (a – g) of Core B (blue circles) and the 7 locations (black triangles) in Table 4 are plotted on a depth scale with zero-depth at Wall Site 3. There is a clear descending trend in the Core B data set, whereas the surface based data set exhibits an opposite trend (see text).

CHEMISTRY

Table 2 presents the mean and the range of the chemical concentrations and the isotope composition in ice from Wall Site 1, 2 and 3 and Core A, B and C. The dominant chemical component is Ca^{2+}, for which concentrations vary 5 to 6 orders of magnitude over the entire Core B (Table 2). The main source for most of the chemical components is the soil where the penetrating precipitation dissolves the minerals. 7 elements: Ca^{2+}, SO_4^{2-}, Cl^-, Na^+, Mg^{2+}, K^+ and F^-, in descending order with respect to concentration levels, have their main origin in this process; whereas NO_3^- has the actual precipitation as a strong contributing source, and NH_4^+ has a strong source inside the cave; the bat drippings.

Recent precipitation in the mountain areas in the vicinity of the Dobšiná Ice Cave contains high concentrations of NO_3^- (in average ~ 30 μeq.·kg^{-1}) and SO_4^{2-}

(in average ~ 100 μeq.·kg^{-1}) (Bodiš, 2000) due to an anthropogenic load of these species into the atmosphere. These concentrations are marked higher than average concentrations in the DIC ice, one order of magnitude in case of NO_3^- and a factor of two in case of SO_4^{2-}. In Greenland ice cores these species have enhanced concentrations over the last 50 – 100 years. There are, however, no signs of increased concentrations in the DIC of NO_3^- and SO_4^{2-} for that period compared to the older parts of the ice core, indicating that these species are interacting with the soil before the precipitation is deposited in the cave.

Fig. 7 presents the Ca^{2+} profile of Core B on a depth scale together with a visual whiteness profile, described below, and the $\delta^{18}O$ profile. The three profiles show high variability, but with apparently no correlation between Ca^{2+} and $\delta^{18}O$. On short terms there are correlations between white bands high Ca^{2+} spikes. In the section of 5.4 to 6 m there is a plateau in the $\delta^{18}O$ record with relatively low values. This plateau is associated with clear ice and low Ca^{2+} concentrations, though there is no direct correlation. Fig. 8 presents the Ca^{2+}, SO_4^{2-} and $\delta^{18}O$

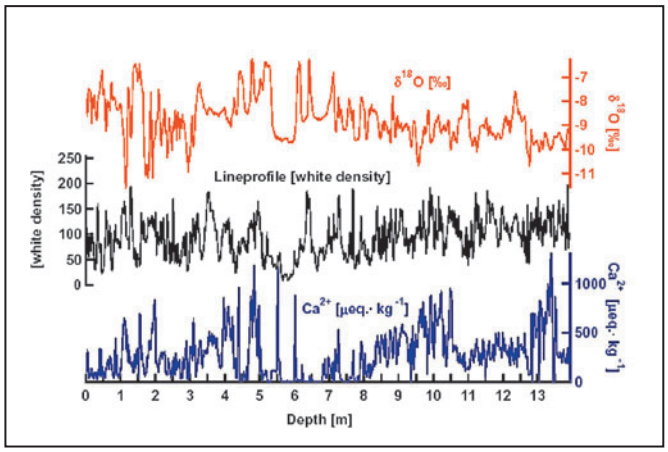

Fig. 7. $\delta^{18}O$, Line Profile and Ca^{2+} concentration along the entire Core B are shown on a depth scale. The units of the three parameters are per mil (red), arbitrary units (black) and equiv.·kg^{-1} (blue), respectively.

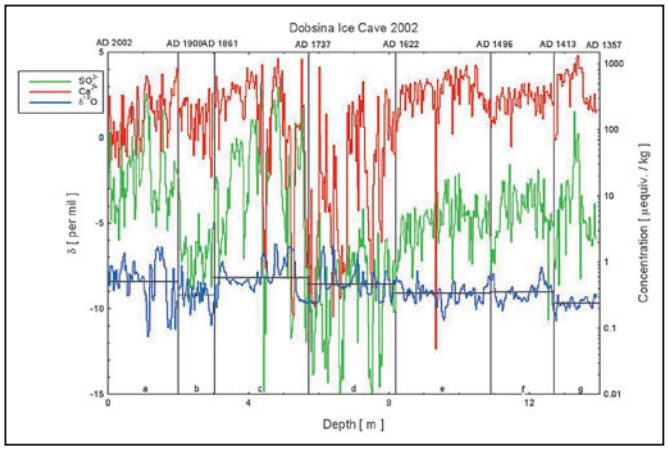

Fig. 8. The concentration levels of Ca^{2+} (red) and SO_4^{2-} (green) are shown on a logarithmic scale versus depth for the entire Core B in 2.5 cm sample resolution. The $\delta^{18}O$ curve (blue) is shown with the mean $\delta^{18}O$ values of the seven sections (a – g), (black). The age intervals corresponding to the seven sections are shown at the top of the graphs.

records of Core B and Fig. 9 presents the NH_4^+, NO_3^- and δD. Both figures show the chemical concentrations on a logarithmic scale. In general there is a high variability in concentrations with high covariance between the different components. It shall be mentioned that a similar general picture is the case for the components not shown here. At around 5.8 m depth, the chemical concentrations increase abruptly and most of the chemical species has marked higher concentrations above this depth than below. This abrupt change occurs in the middle of a plateau in the isotope values and in a large section of clear ice.

CLOUDY BANDS AND BUBBLES

In the DIC ice, laminated features are present along most of the ice core. Brownish dark layers are abundant but cloudy white bands are the most observed feature. The cloudy bands are caused by layers of small bubble-inclusions obscuring the transparency of the ice. A measure of the transparency of Core B is shown on Fig. 7 as a line profile (black curve) based on the photo images of the ice core. The unit of the line profile (white density) is an arbitrary one: low values correspond to clear transparent ice, high values to reduced transparency due to e.g. bubbles, cloudy bands and visible insoluble impurities.

The formation of bubbles is connected to the presence of Ca^{2+} and solid $CaCO_3$ in the water during the freezing process (Žák et al., 2006). As shown in the experiments by Killawee et al. (1998) the initiation of bubble formation during a freezing process will happen when the water reaches Ca saturation. When a shallow water layer freezes rapidly, bubbles will concentrate along the ice-water boundary and through this process layers of small bubbles are formed.

Larger bubbles are also found. These are often part of bubble trails going perpendicular to the cloudy bands. A mechanism for trails is also presented by Killawee et al. (1998). If a chunk of calcite is present in the water during the freezing, bubbles tend to form at one particular place on the piece of calcite. This means that a trail of bubbles will be included in the ice as the ice-water boundary moves downward. The large bubbles are often elongated along the direction of the trails. This can be due to a post depositional temperature effect. If a temperature gradient exists in the ice (warm up - cool down), the ice will sublimate from the warmer top of the bubble and deposit at the cooler bottom ending up with an elongated shape.

CONCLUSION

The mean $\delta^{18}O$ of Core B is -8.39 per mil and the $\delta^{18}O$ values vary between -12 and -6 per mil and the mean value of δD is -58.91 per mil varying between -79 and -39 per mil. On Figs. 8 and 9 are displayed the $\delta^{18}O$ and δD from Core B, respectively, on depth scales. Fig. 8 is provided with our simple time scale at the top of the graph, and a subdivision into time sections ***a-g***. The general

behavior of the two δ-records is identical so what is said for $\delta^{18}O$ is valid for δD. The upper part of the profile (sections ***a*** and ***b*** in Fig. 8) is characterized by high variability. The start in time of section ***b*** corresponds to the time when access to the cave became possible. At the depth level 5 – 7 m are seen large plateaus**.** Plateaus divided by sharp spikes (2 – 3 per mil amplitude) with general low δ-values. The plateaus can be caused by deposition of re-circulated vapour of sublimated cave ice, which will have the mean value of the surface ice. The largest plateau (from 5 - 6 m) may originate from a period when the water flux has been almost completely cut off. The depth interval 5 – 7 m with the most pronounced plateaus corresponds to a time interval of some 100 years from mid 17th to mid 18th century according to the simple timescale. This period is coincident with the cold period in Europe called The Little Ice Age.

The chemistry records of Fig. 8 (Ca^{2+} and SO_4^{2-}) and Fig. 9 (NO_3^- and NH_4^+) show especially in sections ***b*** and ***d*** interesting features. In section ***b*** which corresponds to the time the cave was discovered all components show decreasing concentration levels except for NH_4^+ and the increased NH_4^+ level may be due to increased amount of bat drippings. The chemistry records of section ***d*** which corresponds to The Little Ice Age show large variability with extreme low concentration rates, the level reaches values as low as found in polar ice in Greenland ice cores. These low levels indicate that the ice formed in this period originate from vapor of sublimated cave ice as mentioned above.

Fig. 10 shows in details bubbly, clear and dirty ice in the form of a line profile expressing the transparency of the ice on an arbitrary scale and the crystal sizes. Also shown are the Ca^{2+} and $\delta^{18}O$ profiles over a 38 cm long sequence of Core B in the depth interval 1.62 to 2.00 m, this corresponds to some 20 years centered around AD 1910. The image shows the general picture found along the entire core: high transparency (low white density) corresponds to low Ca^{2+} concentration level and large crystal sizes.

The results of the stable isotope and chemistry measurements of the ice wall samples (Table 2) show that ice cores give useful information that can not be obtained by surface ice wall samples.

CORRELATION OF TEMPERATURE, NAO AND DIC $\delta^{18}O$

Given the special nature of the DIC compared to other ice cores one question is: to what extent does the DIC $\delta^{18}O$ record reflect local temperature changes? Temperature measurements from Vienna are available from AD 1775 AD to AD 1993 (NCDC) and NAO (North

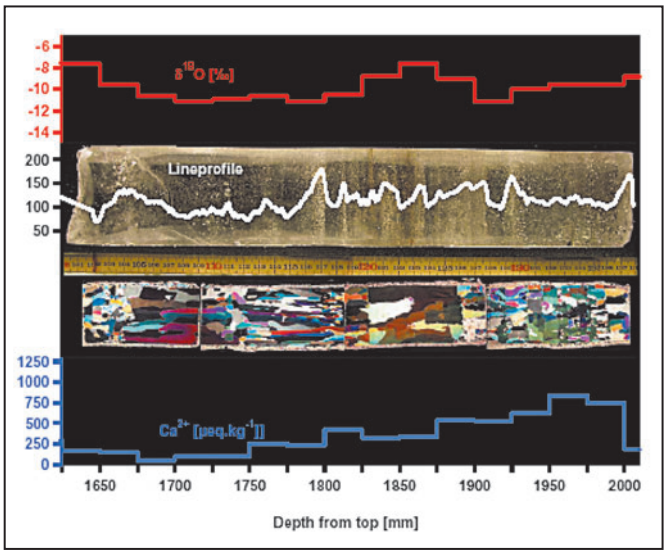

Fig. 10. A 38 cm long ice core section from Core B (1.62 – 2.00 m) is shown with the $\delta^{18}O$ (red) and Ca^{2+} (blue) records along the ice core section. The line profile (a measure of the transparency of the ice) is shown on the photographic image of the core, and below the image is shown the crystal sizes determined in a Rigsby stage.

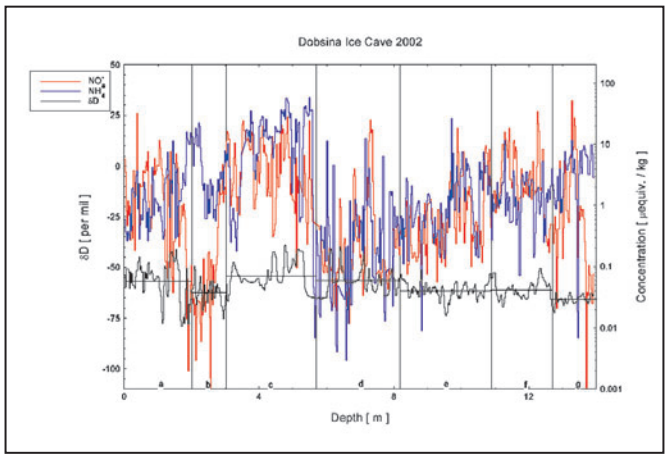

Fig. 9. The concentration levels of NO_3^- (red) and NH_4^+ (blue) are shown on a logarithmic scale versus depth for the entire Core B in 2.5 cm sample resolution. The δD curve (black) is shown with the mean δD values of the seven sections (a – g), (black). The age intervals corresponding to the seven sections are the same as those shown at the top of Fig. 8.

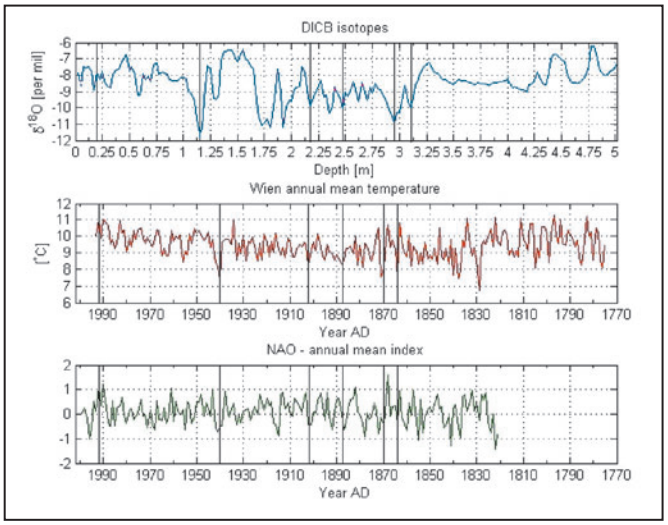

Fig. 11. The annual mean temperature from Vienna since AD 1775, the annual mean index of the North Atlantic Oscillation (NAO) since AD 1832 and the top 5 m of Core B is presented on a linear depth scale. The 5 m depth level corresponds to AD 1770 according to our simple age – depth relationship.

Atlantic Oscillation) from AD 1821 (Vinther et al. 2003). This allows for a feasible investigation to show if the DIC isotopes carry information of temperature and atmospheric variability.

Using both the Vienna temperature and the NAO it is clear that distinct features of these two records also are present in the DIC $\delta^{18}O$. Some peaks in the $\delta^{18}O$ reflect NAO variations more so than temperature and vice versa. The dependence of the $\delta^{18}O$ on the NAO shows that the isotopes also reflect the path of the precipitation accumulated in the cave (Fig. 11, NAO, Vienna temp, $\delta^{18}O$). The direct correlation between temperature and $\delta^{18}O$ is only clear in the top 3 m of DIC. This corresponds to the time period (according to the simple age model) when the cave has had a larger entrance, and consequently a more direct exchange with the surrounding environment. It is also clear that the accumulation of ice in the cave is not constant from year to year, as some features appear stretched while others appear compressed, but a mean annual accumulation rate of ~ 2 cm for the past 100 years is a good estimate.

Acknowledgments

We thank Inger K. Seierstad and Bo Møllesøe Vinter for performing the δD and Remi Chalmas for assisting in the photo documentation of the ice core.

REFERENCES

ARNASON, B. 1969. The exchange of hydrogen isotopes between ice and water in temperate glaciers. Earth and Planetary Science Letters, 6, 423 – 430.

BODIŠ, D. – LOPASOVSKÁ, M. – LOPASOVSKÝ, K. – RAPANT, S. 2000. Chemical composition of snow cover in Slovakia – results of 25-year monitoring (in Slovak). Podzemná voda VI/2000 No.2, p. 162–173.

EDE, H. J. 1908. A Dobsnai Jégbarlang. 1–24.

CRAIG, H. 1961. Isotopic variations in meteoric waters. Science, 133, 1702–1703.

DANSGAARD, W. 1964. Stable isotopes in precipitation. Tellus, 16 (4), 436–468.

GIBSON, J. J. – EDWARDS, T. W. D. 2002. Regional water balance trends and evaporation-transpiration partitioning from stable isotope survey of lakes in northern Canada. Global Biogeochemical Cycles, vol. 16, NO. 2.

HOLMLUND, P. – ONAC, B. P. – HANSSON, M. – HOLMGREN, K. – MÖRTH, M. – NYMAN, M. – PERŞOIU, A. 2005. Assessing the palaeoclimate potential of cave glaciers: The example of the Scărişoara Ice Cave (Romania). Geogr. Ann., 87A (1), 193–201.

KILLAWEE, J. A. – FAIRCHILD, I. J. – TISON, J.-L. – JANSSENS, L. – LORRAIN, R. 1998. Geochimica et Geochimica Acta, 62 (23/24), 3637–3655.

LALKOVIČ, M. 1955. On the problems of ice filling in the Dobšiná Ice Cave. Acta Carsologica, 24, 313–332.

LIEBMINGER, A. – HABERHAUER, G. – PAPESCH, W. – HEISS, G. 2006. Footprints of climate in groundwater and precipitation. Hydrol. and Earth Syst. Sci. Discuss., 3, 271–283.

MICHALKO, J. 1999. Stable isotopes of hydrogen, oxygen and sulphur in waters of Slovakia. Slovak Geol. Mag., 5 (1–2), 63–67.

MORRISON, J. – BROCKWELL, T. – MERREN, T. - FOUREL, F. – PHILLIPS, A. M. 2001. On-line high-precision stable hydrogen isotopic analyses on nanoliter water samples. Anal. Chem., 73 (15), 3570–3575.

VINTER, B. M. – JOHNSEN, S. J. – ANDERSEN, K. K. – CLAUSEN, H. B. – HANSEN, A. W. 2003. NAO signal recorded in stable isotopes of the Greenland ice cores. Geophysical Research Letters, 30 (7), 1387 40–1 – 40–4.

VRANA, K. – BAKER, J. – CLAUSEN, H. B. – HANSEN, S. B. – ZELINKA, J. – RUFLI, H. – OČKAIK, L. – JANOČKO, J. 2007. Continental ice body in Dobšiná Ice Cave – Part I. –project and sampling phase of isotopic and chemical study. This volume.

ŽÁK, K. – ONAC, B. P. – PERŞOIU, A. 2006. Cryogenic formation of carbonate in caves – A review, Archives of Climate Change in Karst. Karst Waters Institute Special Publication 10, 244–247.

NCDC, National Climate Data Centre, data available from site: http://www.wetterzentrale.de/klima/index.html